KnE Materials Science

ASRTU Conference on Alternative Energy
Sino-Russian ASRTU Conference Alternative Energy: Materials, Technologies, and Devices
Volume 2018

Knowledge E
Engaging minds

Conference Paper

Porous Graphitic Carbon Nitride Nanosheets by Pre-polymerization for Enhanced Hydrogen Evolution from Water Splitting under Solar Light

H. Q. Fan, C. Wang, X. H. Ren, and W. J. Wang

State Key Laboratory of Solidification Processing, School of Materials Science and Engineering, Northwestern Polytechnical University, Xi'an 710072, China

Abstract

A facile and green method was developed to fabricate porous graphitic carbon nitride (g-C_3N_4) nanosheets by simple pre-polymerizing melamine. Porous structures were formed in polymerized g-C_3N_4 at 350°C for 2h, which greatly enhanced the specific surface area and pore volume, resulting in superior photocatalytic evolution. The hydrogen evolution rate was 11.2 higher than that of bulk g-C_3N_4 under visible light. The porous structure not only provided abundant active catalytic sites and cross-plane diffusion channels to facilitate the charge and mass transportation, but also promoted the charge separation in the photocatalytic reaction. This g-C_3N_4 is suitable for mass-production to generate hydrogen from water splitting.

Keywords: graphitic carbon nitride, photocatalytic, porous structures, pre-polymerization, hydrogen evolution from water splitting

Corresponding Author:
H. Q. Fan
hqfan@nwpu.edu.cn

Received: 14 September 2018
Accepted: 1 October 2018
Published: 14 October 2018

Publishing services provided by Knowledge E

Selection and Peer-review under the responsibility of the ASRTU Conference Committee.

1. Introduction

Photocatalytic water splitting using semiconductors illuminated with visible light has been considered a green route to utilize the abundant and renewable solar energy. Among the numerous types of photocatalysts used for hydrogen production, graphitic carbon nitride (g-C_3N_4) has shown a great potential for practical applications due to its extraordinary features, such as environmental friendliness, cost-effectiveness, as well as physical and chemical stability. In addition, it has excellent electronic and optical properties. However, the industrial application of g-C_3N_4 is limited by the high recombination rate of photoinduced electron-hole pairs, low specific surface area, and limited active sites [1, 2]. Many approaches have been developed to overcome the deficiencies of g-C_3N_4, such as doping with foreign elements [3, 4], modification with

functional groups [5], manufacturing different g-C_3N_4 nanostructures [6–12], and constructing g-C_3N_4-based nanocomposites [13]. It is well known that g-C_3N_4 could be obtained by condensation of various nitrogen containing precursors (melamine, cyanimide, dicyanamide, urea, and thiourea) at a certain temperature (450–650°C). Recent researches have shown that the precursor could maintain its micro-morphology after polymerization at a relatively low temperature (380–450°C). However, the influence of pre-polymerization in the structure and photocatalytic properties of g-C_3N_4 have not been studied. Herein, we firstly developed a simple pre-polymerization method to obtain porous g-C_3N_4 nanosheets. This method is facile, environment friendly, and does not need any soft or hard template. Remarkably, the g-C_3N_4 pre-polymerized at 350°C exhibits dramatically enhanced photocatalytic efficiency for hydrogen evolution under visible light.

2. Methods

Bulk g-C_3N_4 (CN) was synthesized by direct heating 4g melamine (Me) at 550°C for 4h in air at a ramping rate of 5°C/min. The porous g-C_3N_4 nanosheets were synthesized by a facile pre-polymerization method. First, 4g Me was heated at 350°C for 2h at a ramping rate of 5°C/min. After cooled down to room temperature, the product was ground into fine powder (designated as Me-350). Finally, 2g Me-350 was allowed to fully polymerize at 550°C for 2h at a ramping rate of 5°C/min. After cooling down to room temperature, the product was collected and designated as CN-350. In order to figure out the optimal pre-polymerization temperature, Me was also heated at 300, 400, and 450°C with the following procedure identical to that of Me-350. Here, the obtained products are marked as Me-300, Me-400, and Me-450, in sequence. The resulting g-C_3N_4 are designated as CN-300, CN-400, and CN-450, respectively. The crystal structure was analyzed by powder X-ray diffraction (XRD). The chemical structure was investigated with Fourier transform infrared spectroscopy (FT-IR). The morphology of the photocatalysts was observed by field emission scanning electron microscopy (FE-SEM) and transmission electron microscopy (TEM). The photocatalytic activity of the catalysts was evaluated by hydrogen evolution and degradation of organic dyes under visible light irradiation. In the hydrogen evolution test, 50 mg of catalyst was dispersed in a solution containing 10 mL triethanolamine and 90 mL deionized water. Pt (1 wt%) was in-situ photo-deposited on the catalysts using H_2PtCl_6 as a precursor. The system was evacuated for 5 min to remove air, then irradiated with a 300 W Xeon lamp with a UV cut-off filter ($\lambda > 400$ nm). An external water cooling

circulation system was employed to maintain the temperature of the reactant system at 10°C. The amount of gas evolved was detected by a gas chromatography device. A series of UV-vis filters was applied to test the dependence of hydrogen evolution rate on wavelength.

3. Results

Figure 1 shows the scheme for the synthesis of bulk g-C_3N_4 (CN) and the porous g-C_3N_4 nanosheets (CN-350). CN is synthesized by directly heating Me at 550°C for 4h. For the synthesis of CN-350, Me is first heated at 350°C to pre-polymerize. Then, the pre-polymerized melamine (Me-350) is ground into powder to insure a highly exposed area to the air in the final condensation. Finally, the ground Me-350 is heated to 550°C and kept for 2h to get CN-350. The XRD patterns of Me pre-heated at different temperatures are shown in Figure 2(a). Me-300 displays the same XRD peaks as Me, which means polymerization would not happen at 300°C. The appearance of new peaks in the intermediate products, when Me is heated at 350°C or a higher temperature, is direct evidence of the polymerization process. The intensity of FTIR peaks representing N-H (wave number: 3000–3650) and C-NH_2 bond (wave number: 460–790) for Me-350 (Figure 2(b)) are greatly weakened compared with that of Me. It further indicates that some of the amino groups in Me have been destroyed and the pre-polymerization process would happen, when Me is heated at 350°C. Due to the pre-polymerization process, the ground powder would not aggregate into a macroscopic bulk, but stay in fine powder, when it is heated to 550°C again. Thus, pores are formed, when the pre-polymerized precursor undergoes full polymerization with sufficient exposure to air. The volume of CN-350 sample is about four times larger than that of the CN with the same weight (100 mg), demonstrating that CN-350 becomes fluffy, when a pre-polymerization procedure is introduced before the final condensation process.

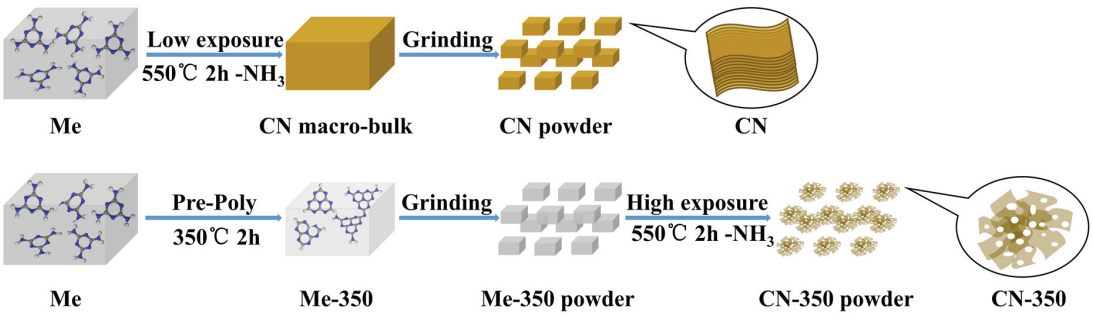

Figure 1: Schematic illustrations of the synthesis process of CN and CN-350.

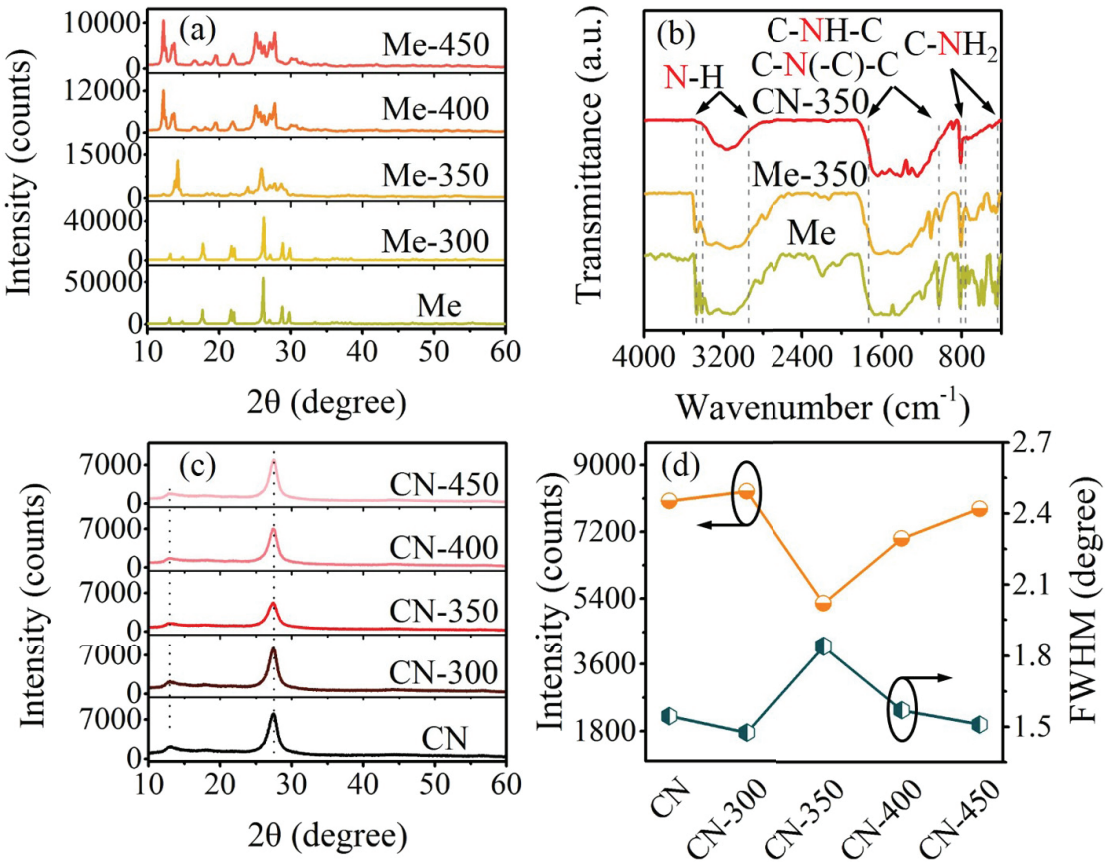

Figure 2: (a) XRD patterns for the pre-polymerized melamine, (b) FTIR spectra for Me, Me-350, and CN-350, (c) XRD patterns, (d) intensity and FWHM of (002) peak for CN and pre-polymerized g-C_3N_4.

The crystal structures of as-synthesized g-C_3N_4 are analyzed by XRD. No shift of the peaks is observed, indicating that the layered structure of g-C_3N_4 is largely preserved in the pre-polymerized samples. Two diffraction peaks at 13.1° and 27.3° in the XRD patterns are ascribed to the in-plane trigonal N linkage of tri-s-triazine units and the stacking of the conjugated aromatic structure, respectively. Interestingly, the intensity and full width at half maximum (FWHM) of (002) peak are greatly changed in the pre-polymerized samples as shown in Figure 2(d). CN-350 shows the lowest intensity and highest FWHM among all the samples, indicating that the long-term order in the stacking of graphitic layers of CN-350 has been greatly weakened. The intensity of the peak at 13.1° is also decreased, which is mainly associated with the large amount of in-plan holes in CN-350 (see the subsequent SEM and TEM images). Change in the XRD characteristics clearly demonstrates that the pre-polymerization procedure can modify the structure of g-C3N4 and exfoliate bulk g-C3N4 into porous nanosheets by a bottom-up method.

The morphology and porous structure of the samples are characterized by SEM. As observed in Figure 3, CN accumulates in dense solid agglomerates with the size of

several micrometers. CN-300 shares similar micromorphology features as that of CN. However, the surface of CN-350 is mostly corroded after the pre-polymerization treatment. In addition, CN-350 is composed of nanosheets with irregular porous structures, which is caused by the final condensation of Me-350, when it is sufficiently exposed to the air and endures a long full-polymerization period. The diameter of pores varies from tens nanometers to several hundred nanometers. It could be noticed that a small amount of porous bulk g-C_3N_4 is also formed in CN-350. However, the surface of the bulk material in CN-350 is much more rough than that in CN and CN-300. The size of the bulk is also much smaller (about 1 μm in the in-plane direction). The sheet-like morphology and rough surface could promise a high specific surface area in CN-350. CN-400 and CN-450 also display a porous trait; besides, the amount of pores is decreased with the rising of pre-polymerization temperature. The porous bulk content becomes predominant in CN-400 and CN-450. In other words, the morphology of the as-prepared g-C_3N_4 turns to porous bulk at a higher pre-polymerization temperature.

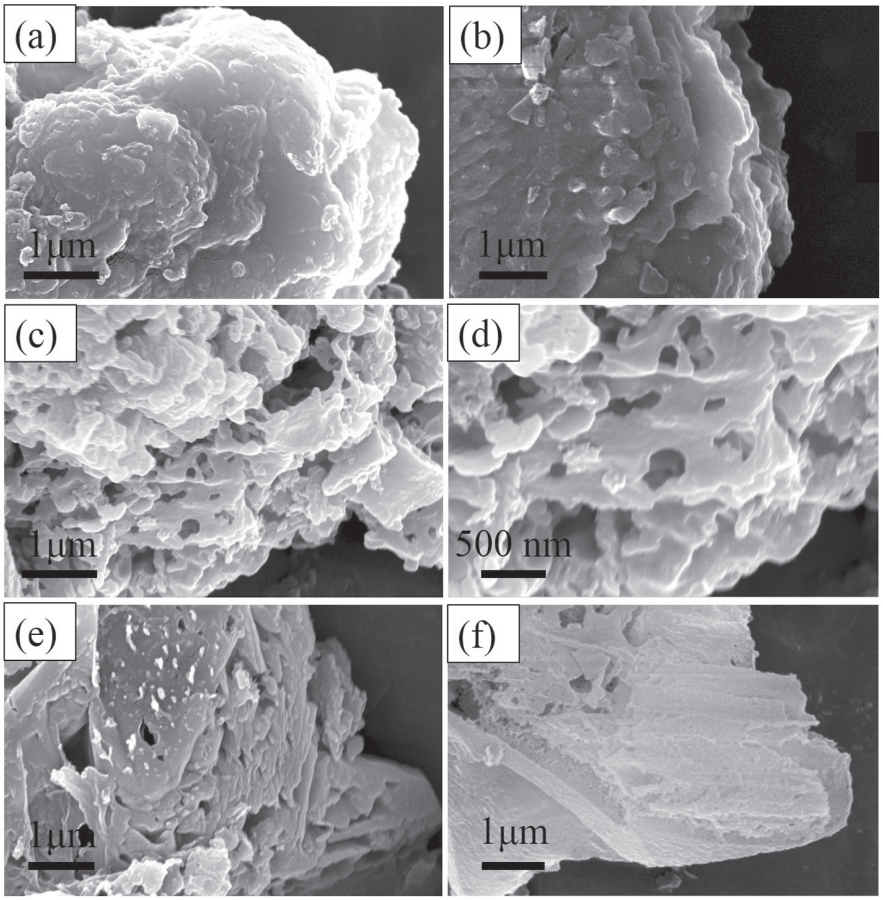

Figure 3: SEM images of (a) CN, (b) CN-300, (c), (d) CN-350, (e) CN-400, and (f) CN-450.

TEM is used for further studying the morphology of the as-synthesized samples. As displayed in Figure 4, CN and CN-300 contain dense stacking layers with flat surfaces,

whereas CN-350 consists of thin layers with curly edges. The enlarged TEM images of CN and CN-350 in Figure 5 clearly demonstrate that pores with a diameter of 20–50 nm can be induced by the pre-thermal treatment of Me. The porous structure in g-C_3N_4 nanosheets could greatly enhance the photocatalytic performance due to the increased exposed active edges. The dark nanosheet morphology declares that CN-450 has thicker stacking layers than CN-400 (Figure 4(e)(f)). It is because Me-400 is less stable than Me-450; thus, it undergoes a longer polymerization process and has more mass loss, when fully polymerized at 550°C.

The photocatalytic performance of the pre-polymerized g-C_3N_4 is evaluated by photocatalytic hydrogen evolution reaction (HER) under visible light irradiation. The photocatalytic H_2 evolution performance of CN and pre-polymerized g-C_3N_4 is displayed in Figure 5(a). CN-350 can produce 349.8 μmol H_2 in 5h, which is 11 times more than that of CN (31.4 μmol). Owing to the porous structure, increased surface area and possibly more abundant active catalytic sites achieved, CN-350 displays much higher photocatalytic activity than CN. The photocatalytic performance of g-C_3N_4 pre-polymerized at different temperature is shown in Figure 5(b). The photocatalytic hydrogen evolution rate of g-C_3N_4 pre-heated at 300, 350, 400, and 450°C is 7.15, 69.69, 53.87, and 37.64 μmol/h, respectively. CN-300 exhibits nearly the same photocatalytic property as CN. It could be ascribed to the fact that melamine is stable at 300°C, thus pre-heating at 300°C has no obvious impact on the structure and photocatalytic performance of g-C_3N_4. CN-350 shows the best performance among all the samples, probably due to the longest polymerization time endured by Me-350, when it is fully condensed to the layered graphitic structure. The photocatalytic performance decreases as the pre-polymerization temperature further rises. A higher pre-polymerization temperature leads to a shorter full condensation process later. Longer full polymerization time promises a higher pore volume, a larger specific surface area, and a better photocatalytic activity. Thus, CN-350 has the best photocatalytic performance among all the samples. The photocatalytic hydrogen evolution performance of CN-350 is superior to most of the recently reported g-C_3N_4. The sustainable capability of CN-350 is evaluated by four consecutive operations, as depicted in Figure 5©. It can be observed that CN-350 displays excellent stability for photocatalytic hydrogen evolution, which shows only a deterioration of 5.4% after four cycles of reaction. The CN-350 photocatalyst collected after four cycles of the photocatalytic reaction exhibits the same crystal structure as that before the reaction. All the aforementioned results proved the excellent recycling performance of CN-350. The HER of CN and CN-350 is also evaluated under a series of irradiation wavelengths (350, 400, 420, 450, 500, and 550 nm) in

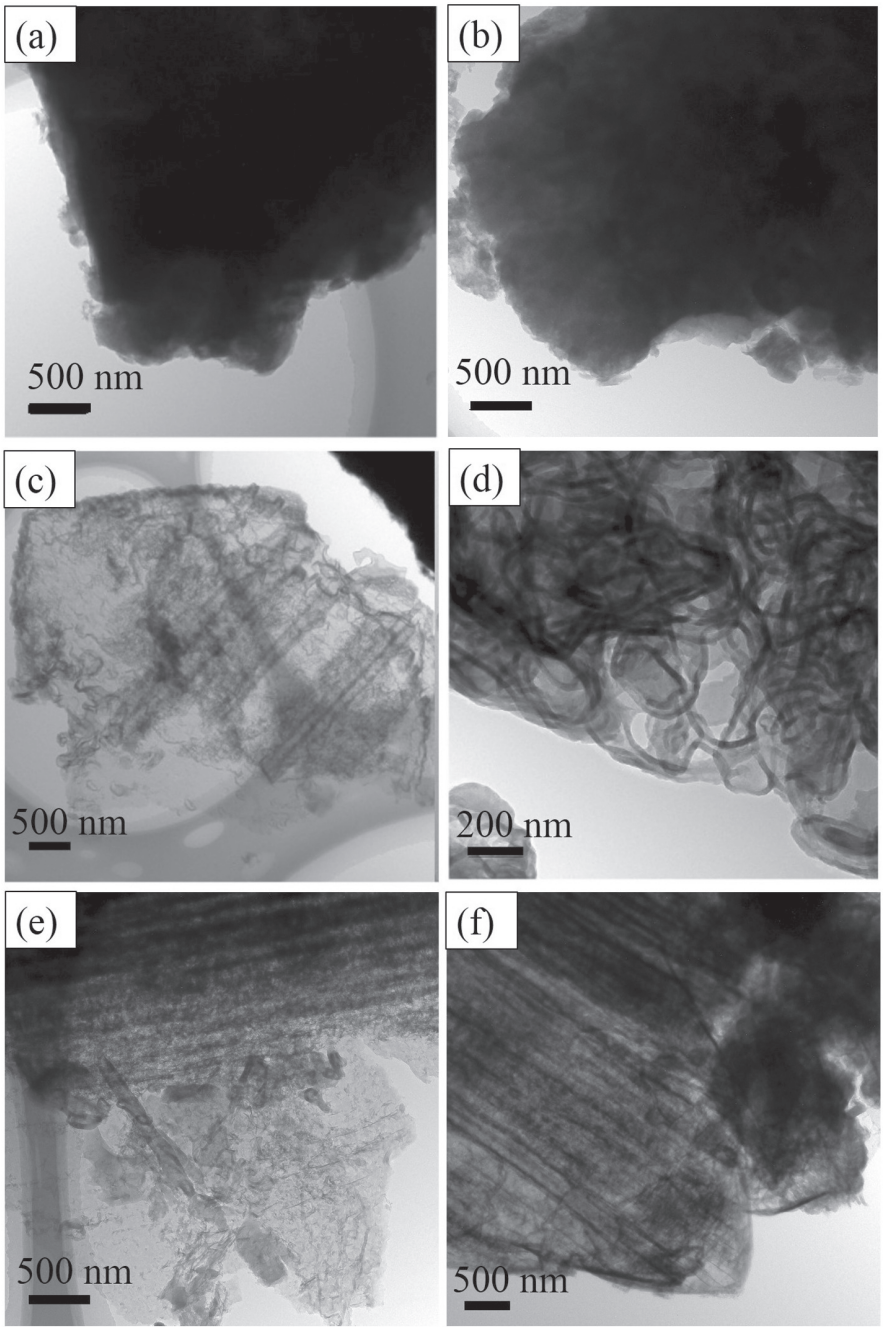

Figure 4: TEM images of (a) CN, (b) CN-300, (c), (d) CN-350, (e) CN-400, and (f) CN-450.

the UV-vis light region. The results show a coincident relationship with the UV-vis absorption spectra, indicating that the absorbed photons are the main driving force for photocatalytic water splitting. The enhanced photocatalytic performance is observed across the whole absorption spectrum in CN-350 catalysts. Interestingly, when the irradiation wavelength reached 450 and 500 nm, the HERs of CN-350 are 2.91 and 0.22 μmol/h, respectively. However, only trace amount of hydrogen can be detected at 450 nm for CN sample and it exhibits no photocatalytic activity at 500 nm. This may

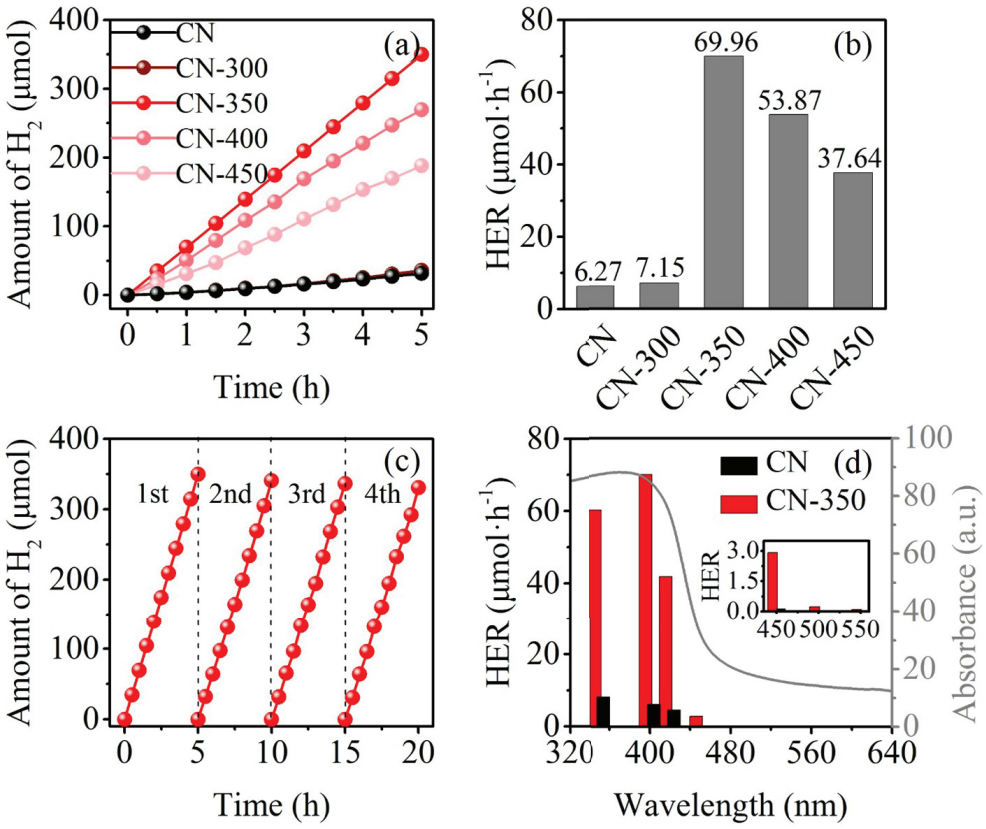

Figure 5: (a) Hydrogen evolution curves, (b) average hydrogen evolution rate of CN and pre-polymerized g-C_3N_4, (c) stability test of CN-350, (d) wavelength dependence of hydrogen evolution rate of CN and CN-350.

be resulted from the multiple-reflection effect and high photoenergy efficiency of CN-350.

4. Conclusion

A porous g-C_3N_4 was synthesized by a simple pre-polymerization method. The porous g-C_3N_4 (CN-350) with a high surface area and a large pore volume exhibited greatly enhanced photo-catalytic performance compared with pristine g-C_3N_4. The enhanced photocatalytic activity was primarily attributed to the increased surface area and the porous structure, which could provide abundant active sites and cross-plane diffusion channels to facilitate the mass and charge transportation. Additionally, this unique structure could improve the electron mobility and suppress the recombination of photo-induced carriers. The CN-350 photocatalyst with high yield, high efficiency, and stable activity, holds great promise in utilizing solar energy for fuel generation and other optical applications.

Funding

This work is supported by the NSFC (51672220) and the NPU Seed Foundation of Innovation and Creation for Graduate Students (Z2018007).

References

[1] Merschjann, C., Tyborski, T., Orthmann, S., et al. (2013). Photophysics of polymeric carbon nitride: An optical quasimonomer. *Physical Review B*, vol. 87, p. 205204.

[2] Algara-Siller, G., Severin, N., Chong, S. Y., et al. (2014). Triazine-based graphitic carbon nitride: A two-dimensional semiconductor. *Angewandte Chemie International Edition*, vol. 53, pp. 7450–7455.

[3] Fang, J. W., Fan, H. Q., Li, M. M., et al. (2015). Nitrogen self-doped graphitic carbon nitride as efficient visible light photocatalyst for hydrogen evolution. *Journal of Materials Chemistry A*, vol. 3, pp. 13819–13826.

[4] Ma, L. T., Fan, H. Q., Li, M. M., et al. (2015). A simple melamine-assisted exfoliation of polymeric graphitic carbon nitrides for highly efficient hydrogen production from water under visible light. *Journal of Materials Chemistry A*, vol. 3, pp. 22404–22412.

[5] Fang, J. W., Fan, H. Q., Zhu, Z. Y., et al. (2016). "Dyed" graphitic carbon nitride with greatly extended visible-light-responsive range for hydrogen evolution. *Journal of Catalysis*, vol. 339, pp. 93–101.

[6] Ma, L. T., Fan, H. Q., Wang, J., et al. (2016). Water-assisted ions in situ intercalation for porous polymeric graphitic carbon nitride nanosheets with superior photocatalytic hydrogen evolution performance. *Applied Catalysis B: Environmental*, vol. 190, pp. 93–102.

[7] Zhao, Y. W., Fan, H. Q., Fu, K., et al. (2016). Intrinsic electric field assisted polymeric graphitic carbon nitride coupled with $Bi_4Ti_3O_{12}/Bi_2Ti_2O_7$ heterostructure nanofibers toward enhanced photocatalytic hydrogen evolution. *International Journal of Hydrogen Energy*, vol. 41, pp. 16913–16926.

[8] Ma, L. T., Fan, H. Q., Fu, K., et al. (2016). Metal-organic framework/layered carbon nitride nano-sandwiches for superior asymmetric supercapacitor. *ChemistrySelect*, vol. 1, pp. 3730–3738.

[9] Ma, L. T., Fan, H. Q., Fu, K., et al. (2017). Protonation of graphitic carbon nitride (g-C3N4) for an electrostatically self-assembling carbon@g-C3N4 core shell nanostructure toward high hydrogen evolution. *ACS Sustainable Chemistry & Engineering*, vol. 5, pp. 7093–7103.

[10] Tian, H. L., Fan, H. Q., Ma, J. W., et al. (2017). Noble metal-free modified electrode of exfoliated graphitic carbon nitride/ZnO nanosheets for highly efficient hydrogen peroxide sensing. *Electrochimica Acta*, vol. 247, pp. 787–794.

[11] Tian, H. L., Fan, H. Q., Ma, J. W., et al. (2018). Pt-decorated zinc oxide nanorod arrays with graphitic carbon nitride nanosheets for highly efficient dual-functional gas sensing. *Journal of Hazardous Materials*, vol. 341, pp. 102–111.

[12] Wang, C., Fan, H. Q., Ren, X. H., et al. (2018). Hydrothermally induced oxygen doping of graphitic carbon nitride with a highly ordered architecture and enhanced photocatalytic activity. *ChemSusChem*, vol. 11, pp. 700–708.

[13] Wang, C., Fan, H. Q., Ren, X. H., et al. (2018). Porous graphitic carbon nitride nanosheets by pre-polymerization for enhanced photocatalysis. *Characterization*,; vol. 139, pp. 89–99.